Catalysis Communications 163 (2022) 106414

Contents lists available at ScienceDirect

Catalysis Communications

journal homepage: www.elsevier.com/locate/catcom

Investigating the preparation of $Cu_3Mo_2O_9$ as a photocatalyst

Nicholas F. Dummer *, Zeenat Sodiq-Ajala, David J. Morgan, Thomas E. Davies

Max Planck- Cardiff Centre on the Fundamentals of Heterogeneous Catalysis FUNCAT, Cardiff Catalysis Institute, School of Chemistry, Cardiff University, Cardiff CF10 3AT, UK

ARTICLE INFO

Keywords:
Copper molybdate
Indigo carmine
Surfactant
Photocatalyst

ABSTRACT

The structural formation of copper molybdate was investigated using a surfactant added during the preparation. The calcined materials were confirmed by XRD to be $Cu_3Mo_2O_9$ and the absorbance band-gap was calculated to be ca. 2 eV. The addition of surfactant resulted in a platelet morphology, in contrast to the agglomerated particles of the standard preparation. Photocatalytic degradation over the catalysts was investigated with indigo carmine. The $Cu_3Mo_2O_9$ catalysts were able to degrade the dye under irradiated conditions. However, the catalyst prepared with surfactant were not as active, although, surface decoration by Cu species was greatly reduced.

1. Introduction

Despite our overall limited access to freshwater, the little that we have is under constant threat [1]. As population size increases, so does the demand for water and issues such as droughts and pollution are the two main causes reducing access to fresh water for many people [1,2]. An unfortunate result of many industries worldwide, including agriculture, pharmaceuticals and textiles, is the pollution of water systems with chemical waste and run offs from production [1]. The textiles industry in particular, causes many issues as it consumes great amounts of freshwater and requires a diverse range of chemicals during processing [3]. There have been at least a million coloured chemical substances that have been produced in the last century with more than 10,000 being commercially available today [4,5]. Around 0.7 million tonnes of dyes are being produced worldwide, of that an estimated 10–20% are released into freshwater systems, whether purposefully or as an unintended consequence this can have damning effects on the life in the surrounding areas [1].

The structures of these dyes can vary greatly, but many have large complicated aromatic systems that make them very stable, and resistant against many of the conventional wastewater treatments [6]. The aromatic groups common in many dyes, such as indigo carmine (IC) are of great concern, as many are synthesised using known carcinogens such as benzidine [3]. Photocatalysts work to produce a continuous flow of $^{\bullet}OH$ and $O_2^{\bullet-}$ radicals to oxidise the waste compounds [7,8]. The oxidising power of various compounds are typically compared to the Normal Hydrogen Electrode (NHE) [9]. The hydroxyl radical (2.8 V), is second only to fluoride (3.0 V) in regards to its oxidising power, as such, utilising photocatalysts in order to generate them, makes for a very powerful tool to use for wastewater treatments, particularly against large, stable, aromatic compounds which can be recalcitrant.

Surfactants have been used successfully to add morphological diversity to many metal oxide formulations through a process of soft-templating. Examples of commonly used soft-templates or surfactants include cetyltrimethylammonium bromide (CTAB) [10], sodium dodecyl sulfate (SDS) [11,12] or block *co*-polymers [13]. The benefits of this diversity can be in directing a morphological change and in turn this can be advantageous if this increases catalytic active site density.

Copper molybdate ($Cu_3Mo_2O_9$), a *p*-type semiconductor, was reported as a visible light-driven photocatalyst [14,15] and has been used for versatile applications such as catalysis [16,17] luminescence and energy storage [14,18–20]. This material has been reported to have a good photocurrent response and the possibility to synthesise various morphologies [14,21]. There have been few reports of the photocatalytic activity of this semiconductor, although it has been shown to degrade Congo red [14] and rhodamine B [22].

The precursor materials were activated and the resultant catalysts characterised to identify the phase, morphology and absorbance band gap. The materials were then evaluated as a photodegradation catalyst, by degrading the common organic dye, indigo carmine, and exploring how the structure of $Cu_3Mo_2O_9$ can be enhanced.

2. Experimental

The material preparation, characterisation and testing methods are detailed in the supplemental information.

* Corresponding author.
E-mail address: dummernf@cardiff.ac.uk (N.F. Dummer).

https://doi.org/10.1016/j.catcom.2022.106414
Received 29 November 2021; Received in revised form 21 January 2022; Accepted 24 January 2022
Available online 26 January 2022

3. Results and discussion

3.1. Material characterisation

The light green coloured copper molybdate precursors CuMoO-STD and CuMoO-SDS, formed by coprecipitation with and without addition of the surfactant SDS, was confirmed to be lindgrenite $\{Cu_3(OH_2)_2(MoO4)_2\}$ by powder XRD (see the supplemental information Fig. S1a). The diffraction patterns of both precursors could be matched to reference file ICDD 01–075-1438. The precursor was then characterised by thermal gravimetric analysis (TGA) under flowing air to determine the temperature at which the oxide forms (Fig. S1b). The phase transition occurs initially at approximately 200 °C and the sharp mass loss ends at 370 °C, overall, the mass loss at 500 °C was ca. 5% for the two samples and this remained relatively stable up to 800 °C. Therefore, 500 °C was chosen as the calcination temperature to ensure formation of the oxide.

Diffraction patterns of the calcined materials CuMoO-STD-C and CuMoO-SDS-C were obtained and were confirmed as $Cu_3Mo_2O_9$ (Fig. 1a). The diffraction peaks were matched to the reference ICDD file 01–070-2493; the reflections at 12.1, 21.6, 23.1, 25.2, 25.9, 27.0, 29.1 and 35.0 degrees 2theta correspond to (020), (130), (200), (131), (002), (140), (112) and (202) respectively. The reflections in the diffraction pattern of CuMoO-SDS-C are broader than those compared to the CuMoO-STD-C. Furthermore, the intensity of the reflections was not consistent when comparing the samples. In particular, the intensity of the (002) reflection at 25.9 degrees 2theta is greater than the neighbouring (131) and (140) reflections for CuMoO-SDS-C and suggests a morphological change. The space group of this orthorhombic structure according to the reference pattern is $Pna2_1$ (33), however, there is a second polymorph of $Cu_3Mo_2O_9$ with the same XRD pattern with the Pnma space group. Recently, Guo and co-workers [18] concluded that only the Pnma phase exists. Our own attempts to resolve this through Rietveld refinement with led to similar fitting with both space group models, as a result we have used the $Pna2_1$ space group in our characterisation as per the ICDD file (Fig. S2). The lattice parameters of the samples were calculated to be $a = 7.68$, $b = 14.62$, $c = 6.86$ Å with a cell volume of 770.56 $Å^3$ for CuMoO-STD-C and $a = 7.67$, $b = 14.62$, $c = 6.87$ Å with a cell volume of 770.36 $Å^3$ for CuMoO-SDS-C, which is close to the 01–070-2493 standard of 769.46 $Å^3$ [23]. Present in the CuMoO-STD-C sample is a broad peak at 38.8 degrees 2theta that was not resolved via Rietveld refinement. We attribute this to a copper oxide impurity, matching the most intense (111) reflection for CuO. Although the reflection overlaps with one of the $Cu_3Mo_2O_9$ reflections a less intense peak is also seen for CuMoO-SDS-C. The presence of CuO crystallites at the surface were confirmed by TEM (Supplementary Fig. S3). The crystallite size of the calcined $Cu_3Mo_2O_9$ samples was estimated with the Scherrer equation as 75 nm and 66 nm from the (020) and (131) reflections, and 35 nm and 39 nm respectively for the CuMoO-STD-C and -SDS-C samples. The specific surface of the calcined materials was measured; CuMoO-STD-C was 3 $m^2\ g^{-1}$ and CuMoO-SDS-C was 13 $m^2\ g^{-1}$.

SEM images of CuMoO-STD-C, suggest that despite a lack of uniformity overall, the agglomerates are made of units with similar dimensions (Fig. 1b). Elemental mapping with SEM-EDX gives a Cu:Mo ratio of ca. 1.3 (Fig. S4) for both materials, which is lower than the expected ratio of 1.5 but consistent with a slight copper deficiency due to CuO impurity formation localised to the surface of the catalyst. TEM-EDX was used to confirm this and a ratio of 1.47 was measured, which suggests some heterogeneity in bulk composition. The TEM images illustrated in Fig. 1d and e highlight the agglomeration of smaller particles of ca. 200 nm diameter for CuMoO-STD-C and the change in morphology resulting in the formation of elongated platelet-type particles for CuMoO-SDS-C. These findings are in contrast to recent work by Keerthana et al., where the addition of SDS was shown to reduce the particle size of $Cu_3Mo_2O_9$, prepared under hydrothermal synthesis conditions at 160 °C for 12 h [24]. Lattice fringe measurements of the

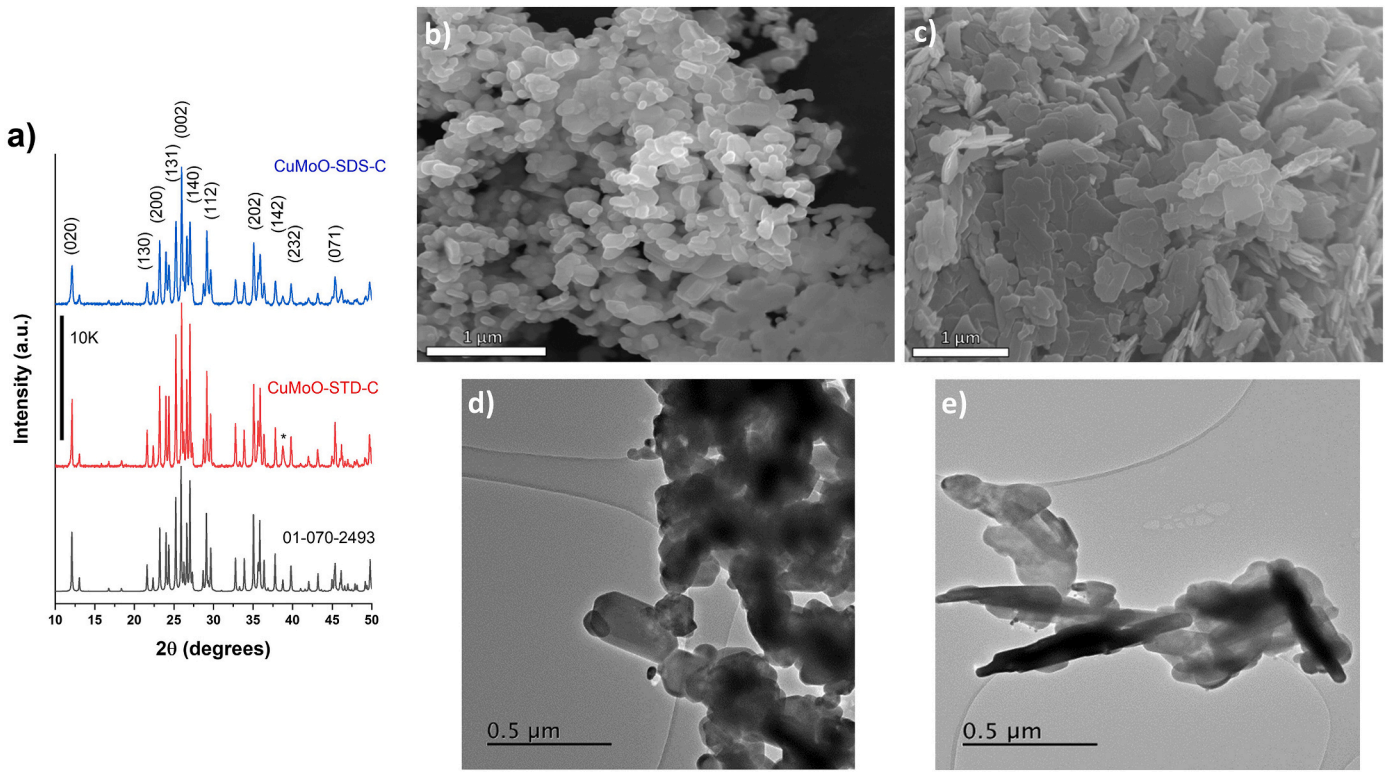

Fig. 1. (a) Powder X-ray diffraction pattern of $Cu_3Mo_2O_9$ calcined at 500 °C for 6 h, which matches the reference pattern ICDD 01–070-2493, reflections are indexed to $Pna2_1$ space group. CuO impurity identified with * at 38.8 degrees 2theta. SEM images of b) CuMoO-STD-C agglomerated particles of ca. 200 nm, (c) CuMoO-SDS-C platelet type particles of ca. 500 nm in length. Transmission electron microscopy of d) CuMoO-STD-C and e) CuMoO-SDS-C.

CuMoO-STD-C catalyst give a spacing of 0.342 nm (Fig. S5) matching the principal reflection (002), given as 0.344 nm (ICDD file 01–070-2493).

Fig. S6 illustrates the XPS survey and Cu(2p) and Mo(3d) spectra for both calcined materials; the corresponding binding energies and at.% concentrations from the high-resolution data are presented in Table S1. For both samples, the Mo(3d5/2) value was found ca. 232.2 eV, consistent with Mo(VI), whilst the Cu(II) component was found at 934.5 (±0.2) eV and confirmed by the presence of the prominent satellite structure between 940 and 950 eV, in general agreement with that in the literature [14,18,25]. The Cu(total):Mo ratio of the CuMoO-STD-C was found to be higher than expected at 1.9, however, the Cu^{2+}:Mo ratio was closer to 1.5 of $Cu_3MO_2O_9$ at 1.6. In contrast, the Cu(total):Mo and Cu^{2+}:Mo ratios for the CuMoO-SDS-C sample were 1.7 and 1.4 respectively. A reduced Cu species with a binding energy of 933.0 (±0.2) eV was also identified. The use of SDS has the potential to result in adsorbed S species, that could poison the catalyst surface. However, no S was found in through XPS analysis. The S(2 s) state overlaps with the Mo(3d) photoemission lines and as Fig. S6 shows and there is no evidence of an extra peak, the S(2p) region is also devoid of signal (Fig. S6).

SEM elemental mapping shows an increased Cu/Mo ratio, whilst XRD closely matches the impurity to CuO found in the diffraction pattern of CuMoO-STD-C (Fig. 1 and Fig. S2). The binding energy of this reduced species sits between bulk values for Cu_2O (932.2) and CuO (933.7) [26] which we ascribe to small islands of Cu_2O on the surface of the material, however, to address the observation of CuO from XRD, one must recall the surface (XPS) vs bulk (XRD) analysis and therefore it is possible a small Cu(I)-containing phase is present at the surface of the molybdate. Analysis of the Cu Auger lines reveal kinetic energy values of 917.1 eV and an associated Auger Parameter values of 1851.6 (±0.2) eV somewhat higher than those for Cu molybdates reported by Haber et al. [25] and supporting a view of mixed Cu phases.

Solid state UV–Vis spectra of the calcined $Cu_3Mo_2O_9$ samples were obtained (Fig. S7) and used to determine the material band-gap. The CuMoO-STD-C sample has absorbance peaks at 253 and 300 nm, with a broad shoulder at ca. 450 nm. These peaks are present in the CuMoO-SDS-C sample although are more defined, with a strong peak ca. 375 nm. Subsequently, Tauc-plots (Fig. S7b and d) were used to estimate the absorbance band-gap for allowed indirect transitions ($r = 2$) and was calculated to be ca. 2.22 eV (CuMoO-STD-C), which is slightly higher than a previously reported value (2.08 eV) [19]. Similarly, for CuMoO-SDS-C the absorbance band gap was calculated to be 2.35 eV. The increased band gap may facilitate more efficient use of UV radiation to complete the transfer of electrons from the valance band.

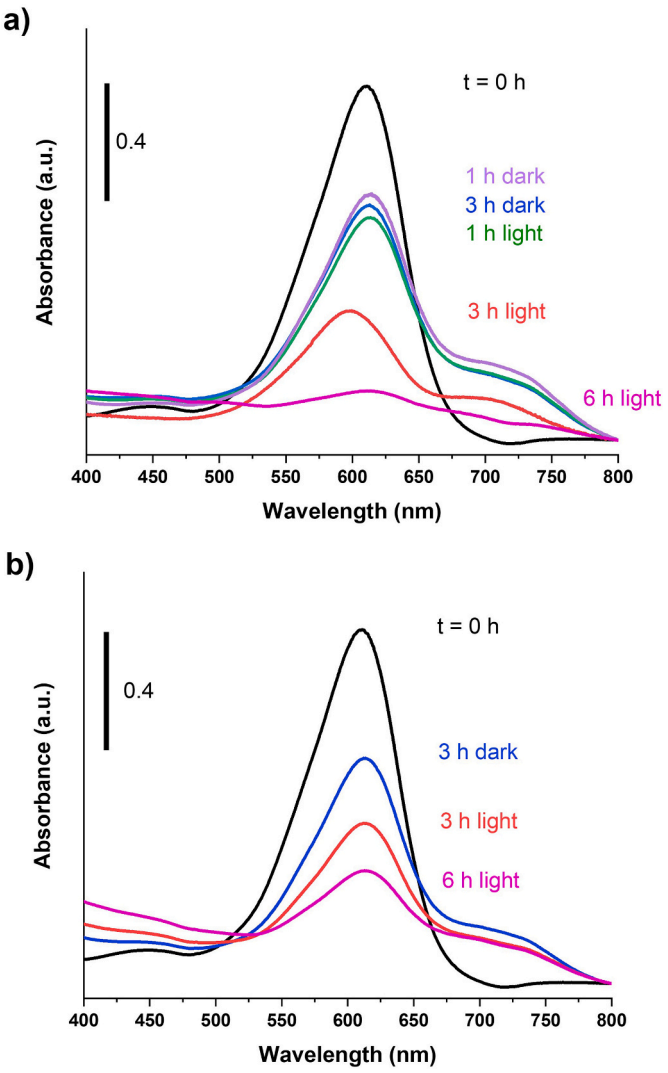

Fig. 2. UV/Vis absorbance measurements of the IC degradation tests over CuMoO-STD-C (a), over CuMoO-SDS-C (b) up to 6 h under light and dark conditions. Reaction conditions; catalyst 50 mg; dye concentration 30 mg l^{-1}, 100 ml, 600 rpm, reaction time does not include 0.5 h pre-reaction stirring under dark conditions.

3.2. Catalyst testing

Copper molybdate was tested in the photochemical degradation of IC under both UV-light (254 nm) and dark conditions following stirring for 30 min under dark conditions. Initially, the dye solution was exposed to UV (6 h), to compare rates of degradation with and without catalyst (Fig. S8). The photodegradation of IC under UV irradiation was greater at 86% over 6 h over CuMoO-STD-C despite a decreased specific surface area, compared to 68% over CuMoO-SDS-C (Fig. 2). Under non-irradiated conditions the initial loss of IC can be ascribed to surface absorption, where the absorbance of IC was decreased by ca. 35% (ca. 1 mg of IC) over both catalysts.

Notably, under light and dark conditions the IC absorbance peak splits into two when catalyst is present, shifting the initial peak bathochromatically slightly and producing a second peak at ca. 705 nm. Furthermore, when IC was reacted over CuMoO-STD-C under UV irradiation (Fig. 2a), the initial peak at 610 nm shifts to ca. 598 nm. However, both peaks gradually decrease over the 6 h reaction period in the presence of catalyst. The experiment was then run without the UV lamp. The peak at 610 nm splits, however, this does not decrease further from 1 to 3 h reaction time, suggesting the UV light is critical to the catalysts ability to degrade the dye. Over the CuMoO-SDS-C catalyst the secondary peak at ca. 705 nm was less pronounced. The concentration of surface Cu that can leach is greatly reduced when SDS was used in the preparation. Cupric oxide (CuO) is a well-known visible-light photocatalyst [27,28], however, the absorbance peak splitting observed over both catalysts suggests that the surface bound CuO is not stable under reaction conditions. We hope to clarify this through subsequent studies involving re-use cycles which should better identify the role of the adventitious CuO.

The leached Cu complicates the degradation of the IC compound, and whilst the reduction in concentration of these species is beneficial, the degradation of IC was decreased. IC is a common dye used to test photocatalysts, although there have been no reports, to our knowledge, that include the splitting of the absorbance peak as a part of the degradation mechanism over other catalysts [29–31]. Zanoni et al. describe the effect of Cu(II) ions in solution on the absorbance of IC [32], and reported that the presence of Cu(II) caused a second peak ca. 715 nm to appear. The second peak is the result of the Cu(II) complexing to the IC compound and it is likely that this occurs, particularly over CuMoO-STD-C as Cu(II) ions may have leached from the catalyst [33]. Post-use XPS analysis indicated that the at.% of the Cu present increased (Table S1), the Cu^{2+}:

Mo ratio increased from 1.6 to 1.8 for CuMoO-STD-C and from 1.4 to 1.5 for CuMoO-SDS-C. We consider the greater change of the STD-C sample is indicative of an increased surface modification, whereas the use of SDS reduced this.

Thermal gravimetric analysis of the catalysts after the tests under light and dark conditions was collected (Fig. S9). The solution contained 30 mg l^{-1} of IC, over CuMoO-STD-C, two minor mass losses were observed, of 0.5% and 3% respectively at ≤100 °C and ca. 330 °C, with an overall mass loss of 4.6% (1.95 mg). A similar loss profile was obtained for the recovered CuMoO-STD-C post-dark reaction, with an overall mass loss of 4.2% (1.63 mg). In contrast, the TGA profiles for the light and dark reactions over CuMoO-SDS-C had a respective overall mass loss of 2.3% and 1.7%, corresponding to 0.19 mg, centred at ca. 305 °C. This could suggest that the retention of reaction species on the surface of the CuMoO-STD-C and -SDS-C are significantly different. It is likely that the first mass loss of STD-C is most likely the loss of adsorbed water (≤ 100 °C), then the decomposition of hydroxyl groups on the surface between 300 and 400 °C, or the decomposition of the partially degraded or whole molecules of the dye. However, the TGA profile is comparable to the precursor transformation (Fig. S1b), potentially, this could lead to greater availability of hydroxyl surface species under reaction conditions and hence increase catalytic activity. The absence of a larger decomposition step with CuMoO-SDS-C, suggests that little of the dye adsorbed to its surface and that the surface was not greatly modified under reaction conditions. We will explore this stability further with reuse experiments in future studies. Suggesting that the photocatalytic reaction follows the first Langmuir-Rideal mechanism, i.e. the hydroxyl radical adsorbed to the surface of the photocatalyst reacts with the free dye molecules in solution.

4. Conclusions

Under standard coprecipitation conditions the $Cu_3Mo_2O_9$ sample comprised of agglomerated particles of ca. 200 nm in size, decorated with CuO nanoparticles. Using a surfactant during the preparation of the precursor resulted in larger, platelet particles and the surface concentration of CuO was reduced according to XRD and XPS analysis. These materials were applied to the degradation of IC which resulted in splitting of an absorbance peak at 610 nm, due to leached Cu(II) complexing with IC. However, despite the leaching, $Cu_3Mo_2O_9$ was able to degrade the dye. Furthermore, the surface of the modified catalyst did not undergo significant surface changes during use. The greater activity of the standard sample can be ascribed to the structural changes providing a greater availability and concentration of hydroxyl species. The use of surfactant resulted in a material with enhanced stability that should have broad appeal to researchers using copper molybdates in a variety of fields such as photocatalysis and energy storage.

Author contribution

NFD conceived the experiments and wrote the manuscript with significant input from all co-authors. NFD and ZS performed the preparation, characterisation and testing experiments and analysed the data.TD captured the electron microscopy images and DMM performed XPS analysis of the materials.

Declaration of Competing Interest

The authors declare that they have no known competing financial interests or personal relationships that could have appeared to influence the work reported in this paper.

Acknowledgements

The authors thank the Max Planck Cardiff Centre and Cardiff University for funding.

Appendix A. Supplementary data

Supplementary data to this article can be found online at https://doi.org/10.1016/j.catcom.2022.106414.

References

[1] K. Rajeshwar, M.E. Osugi, W. Chanmanee, C.R. Chenthamarakshan, M.V.B. Zanoni, P. Kajitvichyanukul, R. Krishnan-Ayer, Heterogeneous photocatalytic treatment of organic dyes in air and aqueous media, J Photochem Photobiol C: Photochem Rev 9 (2008) 171–192.
[2] A. Getirana, Extreme water deficit in Brazil detected from space, J. Hydrometeorol. 17 (2016) 591–599.
[3] T. Robinson, G. McMullan, R. Marchant, P. Nigam, Remediation of dyes in textile effluent: a critical review on current treatment technologies with a proposed alternative, Bioresour. Technol. 77 (2001) 247–255.
[4] I.K. Konstantinou, T.A. Albanis, TiO2-assisted photocatalytic degradation of azo dyes in aqueous solution: kinetic and mechanistic investigations: a review, Appl. Catal. B Environ. 49 (2004) 1–14.
[5] U.G. Akpan, B.H. Hameed, Parameters affecting the photocatalytic degradation of dyes using TiO2-based photocatalysts: a review, J. Hazard. Mater. 170 (2009) 520–529.
[6] W. Chu, Dye removal from textile dye wastewater using recycled alum sludge, Water Res. 35 (2001) 3147–3152.
[7] D. Majumder, I. Chakraborty, K. Mandal, S. Roy, Facet-dependent Photodegradation of methylene blue using pristine CeO2 nanostructures, ACS Omega 4 (2019) 4243–4251.
[8] S. Nagarajan, N.C. Skillen, F. Fina, G. Zhang, C. Randorn, L.A. Lawton, J.T.S. Irvine, P.K.J. Robertson, Comparative assessment of visible light and UV active photocatalysts by hydroxyl radical quantification, J. Photochem. Photobiol. A Chem. 334 (2017) 13–19.
[9] O. Legrini, E. Oliveros, A.M. Braun, Photochemical processes for water treatment, Chem. Rev. 93 (1993) 671–698.
[10] Y.-D. Wang, C.-L. Ma, X.-D. Sun, H.-D. Li, Preparation of nanocrystalline metal oxide powders with the surfactant-mediated method, Inorg. Chem. Commun. 5 (2002) 751–755.
[11] R. Varadharajan, D. Baskaran, Diverse Nano dimension of SDS, PEG and CTAB roofed MgO nano powder synthesized by co-precipitation method, J. Nanostruct. 7 (2017) 189–193.
[12] N.F. Dummer, L. Joyce, H. Ellicott, Y. Jiang, Surfactant controlled magnesium oxide synthesis for base catalysis, catalysis, For. Sci. Technol. 6 (2016) 1903–1912.
[13] H. Chen, J. Yan, Z. Ye, L. Zhang, J. Gao, J. Shi, D. Yan, One pot synthesis of mesostructured non-silica oxides nanocrystallites, J. Mater. Sci. 44 (2009) 6531–6537.
[14] J. Xia, L.X. Song, W. Liu, Y. Teng, Q.S. Wang, L. Zhao, M.M. Ruan, Highly monodisperse Cu3Mo2O9 micropompons with excellent performance in photocatalysis, photocurrent response and lithium storage, RSC Adv. 5 (2015) 12015–12024.
[15] J. Xia, L.X. Song, W. Liu, Y. Teng, L. Zhao, Q.S. Wang, M.M. Ruan, Construction of Cu3Mo2O9 nanoplates with excellent lithium storage properties based on a pH-dependent dimensional change, Dalton Trans. 44 (2015) 13450–13454.
[16] U. Steiner, W. Reichelt, A reinvestigation of Cu3Mo2O9, a compound containing copper(II) in compressed octahedral coordination, Acta Crystallogr. Sect. C 53 (1997) 1371–1373.
[17] M.A. Hasan, M.I. Zaki, K. Kumari, L. Pasupulety, Soot deep oxidation catalyzed by molybdena and molybdates: a thermogravimetric investigation, Thermochim. Acta 320 (1998) 23–32.
[18] J.-C. Li, F. Feng, S.-H. Yang, Y.-R. Gu, H.-G. Xue, S.-P. Guo, Promising electrochemical performance of Cu3Mo2O9 nanorods for lithium-ion batteries, J. Mater. Sci. 52 (2017) 12380–12389.
[19] J. Lv, X. Chen, S. Chen, H. Li, H. Deng, A visible light induced ultrasensitive photoelectrochemical sensor based on Cu3Mo2O9/BaTiO3 p–n heterojunction for detecting oxytetracycline, J. Electroanal. Chem. 842 (2019) 161–167.
[20] B. Saravanakumar, G. Ravi, R. Yuvakkumar, V. Ganesh, R.K. Guduru, Synthesis of polyoxometalates, copper molybdate (Cu3Mo2O9) nanopowders, for energy storage applications, Mater. Sci. Semicond. Process. 93 (2019) 164–172.
[21] J. Xu, D. Xue, Hydrothermal synthesis of lindgrenite with a hollow and prickly sphere-like architecture, J. Solid State Chem. 180 (2007) 119–126.
[22] D.P. Dutta, A. Rathore, A. Ballal, A.K. Tyagi, Selective sorption and subsequent photocatalytic degradation of cationic dyes by sonochemically synthesized nano CuWO4 and Cu3Mo2O9, RSC Adv. 5 (2015) 94866–94878.
[23] L. Kihlborg, R. Norrestam, B. Olivecrona, The crystal structure of Cu3Mo2O9, Acta Crystallogr. Sect. B 27 (1971) 2066–2070.
[24] S.P. Keerthana, B.J. Rani, R. Yuvakkumar, G. Ravi, Y. Shivatharsiny, E.S. Babu, H. S. Almoallim, S.A. Alharbi, D. Velauthapillai, Copper molybdate nanoparticles for electrochemical water splitting application, Int. J. Hydrog. Energy 46 (2021) 7701–7711.
[25] J. Haber, T. Machej, L. Ungier, J. Ziółkowski, ESCA studies of copper oxides and copper molybdates, J. Solid State Chem. 25 (1978) 207–218.
[26] M.C. Biesinger, L.W.M. Lau, A.R. Gerson, R.S.C. Smart, Resolving surface chemical states in XPS analysis of first row transition metals, oxides and hydroxides: Sc, Ti, V, Cu and Zn, Appl. Surf. Sci. 257 (2010) 887–898.
[27] P. Raizada, A. Sudhaik, S. Patial, V. Hasija, A.A. Parwaz Khan, P. Singh, S. Gautam, M. Kaur, V.-H. Nguyen, Engineering nanostructures of CuO-based photocatalysts

for water treatment: current progress and future challenges, Arab. J. Chem. 13 (2020) 8424–8457.
[28] Y. Li, X.-Y. Yang, Y. Feng, Z.-Y. Yuan, B.-L. Su, One-dimensional metal oxide nanotubes, nanowires, nanoribbons, and Nanorods: synthesis, characterizations, properties and applications, Critic. Rev. Solid State Mat. Sci. 37 (2012) 1–74.
[29] A. Gautam, A. Kshirsagar, R. Biswas, S. Banerjee, P.K. Khanna, Photodegradation of organic dyes based on anatase and rutile TiO2 nanoparticles, RSC Adv. 6 (2016) 2746–2759.
[30] M. Vautier, C. Guillard, J.-M. Herrmann, Photocatalytic degradation of dyes in water: case study of indigo and of indigo carmine, J. Catal. 201 (2001) 46–59.
[31] N. Güy, M. Özacar, Visible light-induced degradation of indigo carmine over ZnFe2O4/tannin/ZnO: role of tannin as a modifier and its degradation mechanism, Int. J. Hydrog. Energy 43 (2018) 8779–8793.
[32] T.B. Zanoni, A.A. Cardoso, M.V.B. Zanoni, A.A.P. Ferreira, Exploratory study on sequestration of some essential metals by indigo carmine food dye, Braz. J. Pharm. Sci. 46 (2010) 723–730.
[33] W. Yang, B. Vogler, Y. Lei, T. Wu, Metallic ion leaching from heterogeneous catalysts: an overlooked effect in the study of catalytic ozonation processes, Environ. Sci. Water Res. Technol. 3 (2017) 1143–1151.